Laser and Particle Beams (2003), *21*, 59–64. Printed in the USA.

DOI: 10.1017/S0263034603211125

High-intensity ultrashort laser-induced ablation of stainless steel foil targets in the presence of ambient gas

A. DI BERNARDO,[1] C. COURTOIS,[2] B. CROS,[2] G. MATTHIEUSSENT,[2] D. BATANI,[1] T. DESAI,[1] F. STRATI,[1] AND G. LUCCHINI[1]

[1]Dipartimento di Fisica "G.Occhialini" and INFM, Università degli Studi di Milano–Bicocca, Milano, Italy
[2]LPGP, UMR 8578 Centre National de la Recherche Scientifique Université Paris XI, Orsay Cèdex, France

(RECEIVED 1 March 2002; ACCEPTED 17 October 2002)

Abstract

Ablation depths of stainless steel targets irradiated by 80-fs laser pulses at a flux $F \leq 40$ J/cm^2 (intensity $\leq 5 \times 10^{14}$ W/cm^2) in the presence of air at atmospheric pressure are experimentally measured. These values are lower than the theoretical predictions for metal targets in vacuum. Results are analyzed on the basis of the role of the ambient gas and of crater formation on the behavior of the ablated material.

Keywords: Ultrashort laser; Stainless steel foil targets; Ambient gas; Ablated material

1. INTRODUCTION

In the very recent past, femtosecond lasers have opened new topics (Milchberg *et al.*, 1988; Du *et al.*, 1994; Chichkov *et al.*, 1995; Nemiz, 1995; Preuss *et al.*, 1995; Lenzer *et al.*, 1998) in the study of surface processing of metals, polymer, dielectrics, of thin film deposition, surgery, micropacking, fast ignition (Hall *et al.*, 1998; Batani *et al.* 2000; Pisani *et al.*, 2000; Santos *et al.*, 2002) and even of the dismantling of the atomic weapon stockpiles, besides the study of fundamental aspects of laser plasma interaction. There have been several reports on the study of physical properties like electrical resistivity (Nemiz, 1995), laser induced surface breakdown (Du *et al.*, 1994; Nemiz, 1995; Stuart *et al.*, 1995), plasma temperature (Milchberg *et al.*, 1988; Ng *et al.*, 1995), and so forth for plasmas produced by femtosecond lasers.

Femtosecond lasers have also been used for the fabrication of debris-free microstructures with high precision (Preuss and Stuke, 1995; Chichkov *et al.*, 1996). Subpicosecond lasers provide optimum energy deposition in a minimized volume of the target material because energy spreading from the heated zone and plasma shielding due to vaporization occur on a time scale significantly longer than the laser pulse duration. After the laser pulse has passed, damage and ablation take place in a volume primarily determined by the energy penetration depth (Kautek & Kruger, 1996). Due to ultrashort duration, femtosecond lasers offer several advantages to the study of material processing: (1) laser energy is rapidly deposited on the target surface due to inverse bremstrahlung because of high collision frequency at solid density, (2) hydrodynamic expansion of the material ablated from the target surface is negligible during the laser pulse, and (3) thermal diffusion to the surrounding material is negligible, leading to a lower ablation threshold and the absence of molten material (Kanavin *et al.*, 1998; Lenzer *et al.*, 1998).

In vacuum, the target material ablates with no adverse effect from the surrounding gas; instead the presence of an ambient atmosphere may significantly reduce ablation due to redeposition of ablated material (Preuss *et al.*, 1995; Nolte *et al.*, 1996; Lenzer *et al.*, 1998). Thus the size and shape of the ablation site will depend on laser parameters (wavelength λ, pulse duration τ, and laser flux F) and on the physical and chemical characteristics of the target material, but also on the ambient atmosphere (gas pressure and gas properties). Therefore, a proper choice of the ablation conditions is necessary for each type of material in order to optimize the ablation process.

The main goals of the experiment presented in this article were to study the ablation of metal targets from femtosecond lasers at higher intensities ($I \leq 5 \times 10^{14}$ W/cm^2) than those previously reported in the literature, and in the presence of an ambient gas. Therefore laser drilling of stain-

Address correspondence and reprint requests to: A. Di Bernardo, Dipartimento di Fisica "G. Occhialini" and INFM, Università degli Studi di Milano-Bicocca, 20126 Milano, Italy.

less steel foil targets was performed in air at atmospheric pressure without using any vacuum chamber. Several reports are available about drilling a flawless and debris-free microstructures using femtosecond laser beams (Preuss *et al.*, 1995; Nolte *et al.*, 1996; Lenzer *et al.*, 1998). When the quality of the ablated site and surface finish are not the prime criteria in drilling a hole in a metal target, one can do so at high intensity and in air without using any vacuum chamber and evacuation accessories. This study also has practical applications when the target dimensions are too large to accommodate in a vacuum chamber.

2. EXPERIMENTAL SETUP

Experiments were performed at the Laboratoire d'Optique Applique (LOA) in Palaiseau, France, using a dye laser of wavelength $\lambda = 620$ nm and pulse duration $\tau \approx 80$ fs (FWHM) with a repetition rate of 10 Hz and energy per laser pulse up to 3 mJ. However, in the present experiment, $\approx$60 μJ of laser energy were delivered onto the target surface. The laser focal spot diameter was also varied from 13 μm to 30 μm. Then a laser flux F on the target surface between 2 and 40 J/cm^2 was obtained. Laser energy reproducibility from shot to shot was of the order of $\pm$10%. Maximum laser intensity on the target surface was $\approx 5 \times 10^{14}$ W/cm^2. A stainless steel foil target of thickness 120 μm was irradiated in air with laser light at normal incidence on the target surface. A shutter placed on the laser beam allowed us to choose the required number of pulses for target irradiation. Ablation depth for a given laser flux was measured by exposing the ablation site with 1000 laser pulses. Quantitative measurements of ablation depth were then performed using an optical and a scanning electron microscope. Ablation depth per shot was estimated as the total ablation depth (measured value) divided by number of shots (1000).

3. EXPERIMENTAL RESULTS

Our experimental results are summarized in Figure 1, which represents the ablation depth per single shot in a stainless steel target, as a function of incident laser flux F. Ablation depth increases with laser flux F, but at fluxes higher than $F \approx 5$ J/cm^2, the increase becomes slower. In other words, higher laser fluxes (higher intensities) seem to be less effective in mass ablation. Images of the ablated sites are shown in Figure 2. In particular, Figure 2a,b show, respectively, the ablation site for 1000 laser shots at $F = 9.8$ J/cm^2 and at 105 J/cm^2. We notice that the morphology of the ablation site shows cracks, blobs of molten material, ripples, and so forth around the irradiance site as in Figure 2a and this increases with increasing laser flux as in Figure 2b. The rear side of the ablated site is relatively free from such adverse effects, as shown in Figure 3.

4. COMPARISON WITH THEORETICAL MODELS

Ablation depth is estimated theoretically by various authors (e.g., Eesley, 1986; Groeneveld *et al.*, 1990) in the optical penetration regime, and at higher fluxes, in electron heat conduction regime, by Nolte *et al.* (1996). Figure 1 also represents the theoretical values of ablation depth per shot as given by Eq. (1) below, according to the model described by Nolte *et al.* (1996)

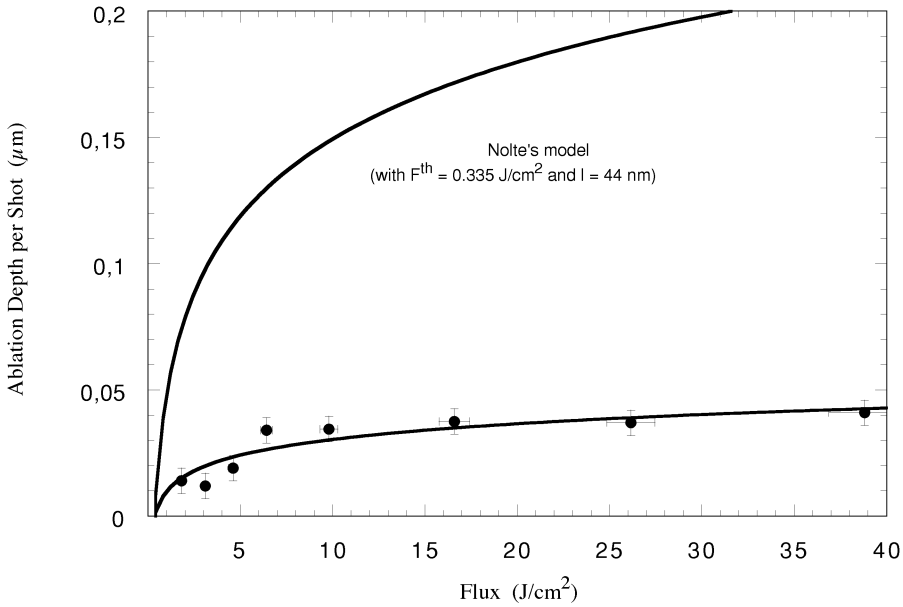

Fig. 1. Ablation depth (μm) per pulse as a function of laser flux F (J/cm^2) on the target surface. Experimental results (black circles) are compared (a) with an interpolation corresponding to the formula L (μm) = 9 ln(F/0.335), and (b) with Nolte *et al.*'s (1996) formula.

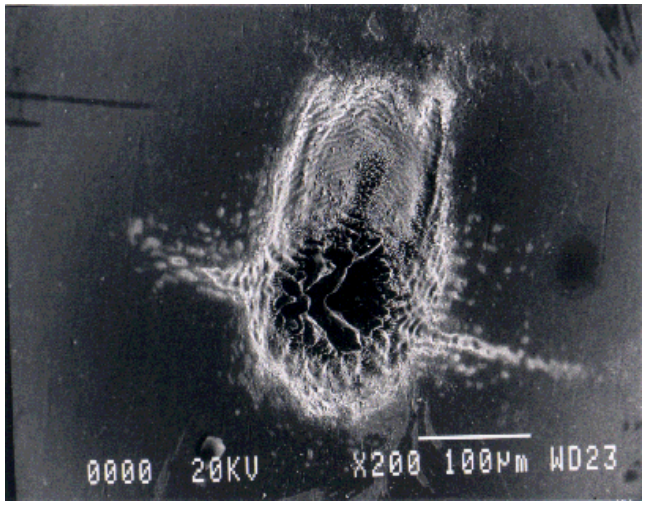

(a)

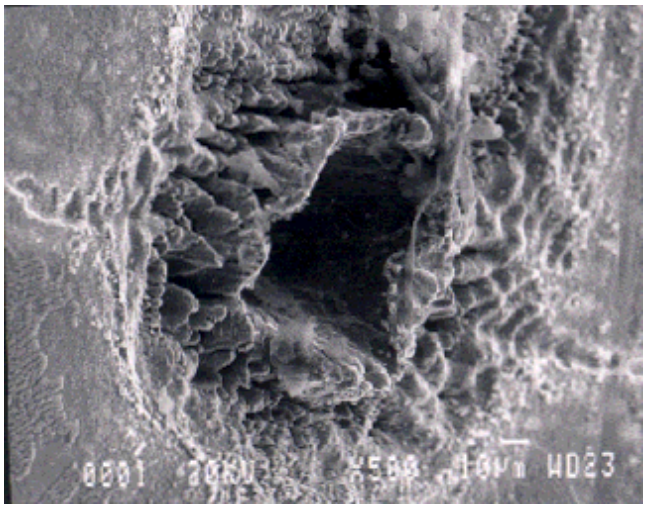

(b)

Fig. 2. Front surface of the ablation site after exposing the target surface with 1000 laser pulses at $F = 9.8$ J/cm^2 (a), and $F = 105$ J/cm^2 (b).

$$L = l \ln(F/F_{th}), \tag{1}$$

where L is the ablation depth per pulse, F is the laser flux on target surface, and F_{th} is the threshold flux. l is the typical energy penetration depth, which Nolte *et al.* (1996) identify with the optical penetration depth $= c/\omega_p$ at low fluxes ($F <$ 0.5 J/cm^2), and with the electron heat penetration depth $= a(M_i/3m_e)^{1/2}$ at higher fluxes. Here a is the average interatomic distance, and M_i and m_e are ion and electron mass, respectively. The threshold flux is given by $F_{th} = \rho\Omega l$ where ρ is the density and Ω the specific heat of evaporation per unit mass of the material, respectively. The threshold flux is calculated when the energy of the lattice ($C_i T_i$) exceeds the heat of evaporation $\rho\Omega$, where C_i is the heat capacity of the lattice per unit volume and T_i is the ion temperature. In our case, we consider the values of iron since stainless steel

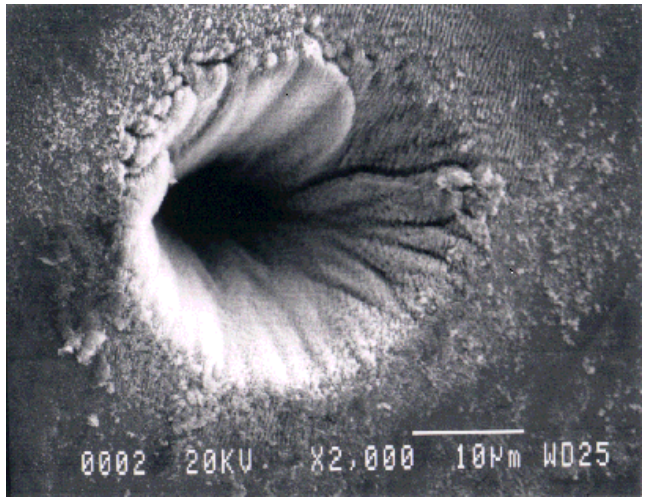

Fig. 3. Rear surface of the ablation site after exposing the front surface to a number of laser pulses sufficient to get complete drilling at $F =$ 33.6 J/cm^2.

contains 97% iron. Hence $\rho = 7.8$ g/cm^3 and $\Omega = 7482$ J/g. From iron data (Samsonov, 1968) we also calculate that l(optical) = 18.3 nm and l(conduction) = 41.9 nm. This gives threshold fluxes of 0.1 J/cm^2 and 0.24 J/cm^2, respectively, for the optical and electron heat penetration regimes. The threshold for laser ablation has also to be divided by surface absorptivity (Nolte *et al.*, 1996). This is ≈33% for an iron surface at normal incidence (Landsberg, 1976). Metal reflectivity will rapidly change during laser irradiation (Milchberg *et al.*, 1988). However this will influence the ablation depth only very weakly due to the logarithmic dependence of Eq. 1. Thus we can conclude that F_{th} for laser ablation in our case at high fluxes is ≈0.335 J/cm^2.

Eq. (1) has been used by Nolte *et al.* (1996) to explain their experimentally observed ablation depths for a copper target irradiated by 150-fs, 30-ps laser pulses in vacuum. In our case, the laser flux is high. Therefore electron heat conduction is the most important mechanism of energy transport and the electron heat transport regime can be applied to our results in order to discuss the effect of the ambient gas on the ablation depth. However, Figure 1 shows that Eq. (1) largely overestimates experimental results. For comparison, we have also drawn the interpolation of our experimental results with a formula of the type $L = l \ln(F/F_{th})$ where we used the value $F_{th} = 0.335$ J/cm^2 previously calculated and we left l as a free interpolation parameter. The best fit gives $l = 9$ nm. The experimental values are interpolated fairly well by this formula, showing a strong reduction in l (≈4.6 with respect to the calculated value), which accounts for the strong decrease in ablation depth. Let us observe that the evaluation of threshold from experimental data (Fig. 1) is difficult due to the logarithmic dependence of Eq. (1). Also it is not possible to reduce the flux on the target to get a better evaluation of F_{th} because this would bring us in a different regime (optical penetration).

5. DISCUSSION

There could be several reasons for the observed reduction in ablation depth: (1) Presence of air envelope, (2) Decrease of laser flux with increasing ablation depth, (3) Increase in material density due to laser induced shock compression, (4) Confinement of ablated material in the crater and condensation, and (5) Radiation transport effect.

5.1. Effect of Air Envelope

Although the expansion of the ablated material during the laser pulse is negligible, expansion persists after the laser pulse due to conversion of thermal energy in kinetic energy of the plasma. Motion of the ablated material is constrained due to the presence of the envelope of the ambient gas, which will lower the plasma velocity compared to free expansion of plasma in vacuum. Presence of ambient gas offers a mechanical resistance to the free flow of the ablated material. The ablated material will recombine and also cool off rapidly as it expands in a span of approximately nanoseconds, implying that a fraction of the ablated material will condense in the vicinity of the ablation site. Ablated material also condenses in and around the ablation site before the arrival of the next pulse ($\sim$0.1 s). This causes a reduction in ablation depth and it is also one of the reasons for the appearance of the molten material at the edge of the ablation site, as seen in Figure 2. A similar observation has been reported by Gupta *et al.* (1991) in their study on fragments produced by laser ablation: The fragments did not leave the target surface when an ambient gas at sufficiently high pressure is present.

The ablation rate will be decreased by the fraction of material that redeposits on the ablation site and this depends on the pressure and nature of the ambient gas as well as on focal spot characteristics (Preuss *et al.*, 1995). In a similar way, the motion of the blowoff material from the walls is reduced in gas-filled hohlraums used in indirect drive inertial fusion energy experiments due to the presence of ambient gas, and higher density gas holds back the plasma for a longer time (Delamater *et al.*, 1996).

5.2. Increase in Irradiation Area

With multiple laser shots, ablation depth increases and the effective laser irradiated surface becomes larger. In particular, for a hemispherical structure $L \approx R$ (focal spot radius), the laser irradiated surface area increases by twofold, causing a reduction in laser flux to half of its original value. Thus, the actual laser flux has to be accounted for, and for large values of L, Eq. (1) can be written as

$$L = l \ln(F\pi R^2/AF_{th}), \tag{2}$$

where A is the actual laser irradiated area and R and F are initial focal spot radius and laser flux. This effect is expected to be larger at higher fluxes, which corresponds to the larger depths and for a large number of laser shots. For instance, in the case of irradiation at 40 J/cm^2, after 500 laser shots, from Figure 1, the ablation depth is $(0.035 \times 500) \approx 17$ μm, that is, of the same order of focal spot size. Hence we expect an increase of the irradiated area of the order of $A/\pi R^2 \approx 2$. However, this effect is not large; due to the logarithmic dependence of the ablation depth, this only implies a reduction of about 15% in ablation rate.

5.3. Shock Compression

Laser-irradiated targets also experience shock compression. A shock wave is generated due to recoil of the ablated material in the direction of laser, and this compresses the solid material to a higher density (Koenig *et al.*, 1999; Batani *et al.*, 2000, 2002). The maximum increase in density corresponding to a single strong shock is $(\gamma + 1)/(\gamma - 1) = 4$, where $\gamma = (Cp/Cv) = 5/3$. Strength of the shock compression depends on laser flux. For a given laser intensity of $\approx 10^{14}$ W/cm^2, ablation pressure (Lindl, 1995) is $\approx$15 Mbars, and the corresponding compressed material density is $\approx$ 18.7 g/cm^3 using the well-known Sesame tables (Sesame report, 1983). The real resulting compression before the following laser pulse (in our series of 1000 shots) is not known since after such peak compression the material will experience some relaxation and decompression. However, some residual compression will remain, laser shocks are indeed used for surface compactification (Fournier, 1989), implying a decrease in interatomic distance and thus in the parameter l ($\approx a$). This results in the decrease of ablation depth. Again, however, this effect is not dominant: Assuming irradiation at 40 J/cm^2 and a factor of $\approx$2 in material compression brings a reduction of about 30% in ablation rate, which is important, but small compared to the observed reduction in l (a factor of $\approx$4.6).

5.4. Confinement of Ablated Material in the Crater and Condensation

After irradiation on the target surface, especially for successive laser pulses, a crater is formed and the plasma may be effectively confined inside if its depth is larger than the distance to be traversed by the ablated material (within its condensation time $\tau_c \approx 1$ ns). This reduces the efficiency of ablation. The minimum saturated ablation depth in vacuum can be roughly calculated assuming the plasma flow inside the crater remains one dimensional, and this can be determined by the condition $L_{sat} \geq C_s\tau$ where C_s is plasma velocity in vacuum corresponding to laser flux on the target surface, $C_s = (Z^*KT_e/M)^{1/2}$, where T_e is plasma temperature, Z^* the effective plasma ionization, and τ is laser pulse duration. Time-resolved dynamics of laser ablation irradiated by a 500-fs duration laser pulse has been reported by Preuss *et al.* (1993). According to their study, the ablation rate is very sensitive to the time delay between the two pulses. With their measurements for a long delay time $>$50 ps,

ablation rate for two consecutive pulses is equal to that obtained by a single pulse, whereas for < 50 ps, the ablation rate increases with decreasing delay.

For femtosecond laser-produced plasmas, electron temperature will be, in general, higher than ion temperature. Ng *et al.* (1995) have studied the formation and propagation of heat fronts produced by intense femtosecond laser pulses in solids using one-dimensional numerical calculations which treat self consistently the process of laser absorption, electron thermal conduction, and hydrodynamics. The maximum plasma temperature at $I \approx 10^{15}$ W/cm^2 for a 500-fs laser was estimated as ≈100 eV. An electron temperature of a similar order for an aluminum target irradiated by 400-fs laser pulses has been reported by Milchberg *et al.* (1988). In our case, taking into account the smaller intensity and the different material, we can estimate a temperature of a few tens of electron volts, which yields a saturated ablation depth L_{sat} of the order of a few tens of microns.

5.5. Radiation Transport

Kanavin *et al.* (1998) have pointed out that in principle at high laser fluxes, radiative heat transfer could influence ablation depth. Radiative transport is an important mechanism of energy carrier over thermal conductivity, provided the conduction zone ($n_c < n_e < n_s$) is optically thick (a near Planckian condition) and is efficiently emitting X rays. For a black body flux, the coefficient of radiation conductivity (Zeldovich & Raizer, 1967) is given by $K_R = [16\sigma\lambda_R(T_R)^3]/3$, where σ is the Boltzmann constant $= 5.67 \times 10^{-5}$ ergs/s·cm^{2}K, T_R is the black body radiation temperature, and λ_R is the radiation mean free path. This can be calculated as the Rosseland mean free path (Zeldovich & Raizer, 1967) for bound-free transition, or $\lambda_R = [4.4 \times 10^{22}(T_k)^{7/2}]/[Z^*(Z^*+1)^2 n_i^2]$ cm, where T_k is in degrees Kelvin. In our experimental conditions, assuming again a temperature of a few tens of electron volts, a calculation of radiation conductivity yields a value which is comparable to electron thermal conduction. Thus, in our case, such an effect is not going to drastically affect our conclusions.

6. CONCLUSIONS

Ultrashort ultrahigh intensity laser-induced ablation of stainless steel targets in the presence of air at atmospheric pressure shows a lower ablation rate compared to vacuum. This can happen if one or more phenomenon discussed above occurs simultaneously during the ablation of the target material. With our present knowledge it is not possible to quantify the contribution of each of these processes in reducing the ablation depth exactly. However the previous discussion suggests that phenomena 2 (increased irradiation area), 3 (shock compression), and 5 (radiation transport) are not very important. Finally the fact that we can reproduce our data with a single Nolte-like formula, without any changes at higher fluxes, seems to suggest that the main effect is redeposition induced by the pressure of air. Indeed crater structure could be more effective for deeper craters and hence at higher fluxes.

The ablated site (Fig. 2) very clearly shows a nonuniformly heated region with cracks, blobs of ablated material, and ripples around the focal spot. The effect is more pronounced at higher laser flux (Fig. 2b). Contrary to this, Figure 3 shows the rear side of the ablated surface. A through hole was drilled with $F = 33.6$ J/cm^2 in the entire target thickness (120 μm) with several laser pulses. Here a clean central hole is evident with damaged surroundings. This also seems to confirm that the front surface effects are indeed due to redeposition of the ablated material.

We believe the appearance of molten material and blobs at the edge of the ablation site is mainly due to the presence of air. It is well known that in vacuum, with femtosecond laser pulses, thermal diffusion is significantly reduced, and hence no molten material appears in and around the ablated region. The presence of air impedes the free expansion of the ablated material. For metals, part of the laser-evaporated material can then be redeposited on the surface in and around the ablation site.

Condensation of molten material around the ablation site is unfavorable for producing fine and debris-free microstructures in materials processing. Nevertheless, a practical advantage of the work reported here is that this is a less expensive technique for drilling deep microholes in large-dimension targets at atmospheric pressure without using any vacuum chamber.

ACKNOWLEDGMENT

We warmly acknowledge the support of the staff at LOA, Palaiseau, France.

REFERENCES

Batani, D. *et al.* (2002). *Phys. Rev. Lett.* **88**, 235502.
Batani, D. *et al.* (2000*a*). *Phys. Rev. E* **61**, 5725.
Batani, D. *et al.* (2000*b*). *Phys. Rev. B* **61**, 9287.
Chichkov, B.N. *et al.* (1996). *Appl. Phys. A* **63**, 109.
Delamater, N.D. *et al.* (1996). *Phys. Plasmas* **3**, 2022.
Du, D. *et al.* (1994). *Appl. Phys. Lett* **64**, 3071.
Eesley, G.L. (1986). *Phys. Rev. B* **33**, 2144.
Fournier, J. (1989). *Generation d'ondes de choc par laser pulse de forte energie: Applications mecaniques et metallurgiques*, Ph.D. Thesis, Ecole Polytechnique, Palaiseau, France.
Groeneveld, R.H.M. et al. (1990). *Phys. Rev. Lett.* **64**, 784.
Gupta, A. *et al.* (1991). *Appl. Phys. Lett.* **59**, 1302.
Hall, T. *et al.* (1998). *Phys. Rev. Lett.* **81**, 1003.
Kanavin, A.P. *et al.* (1998). *Phys. Rev. B* **57**, 14698.
Kautek, W. & Kruger, J. (1996). *Appl. Phys. Lett.* **69**, 3146.
Koenig, M. *et al.* (1994). *Phys. Rev. E* **50**, R3314.
Landsberg, G.S. (1976). *Optics* (p. 85), Moscow: Mir Publishers.
Lenzer, M. *et al.* (1998). *Phys. Rev. Lett.* **80**, 4076.
Lindl, J. (1995). *Phys. Plasmas* **2**, 3933.
Milchberg, H.M. *et al.* (1988). *Phys. Rev. Lett.* **61**, 2364.
Nemiz, M.H. (1995). *Appl. Phys. Lett.* **66**,1181.

Ng, A. *et al.* (1995). *Phys. Rev. E* **51**.
Nolte, S. *et al.* (1996). *J Opt. Soc. Am. B* **14**, 2716.
Pisani, F. *et al.* (2000). *Phys. Rev. E.*
Preuss, S. *et al.* (1993). *Appl. Phys. Lett.* **62**, 3049.
Preuss, S. *et al.* (1995). *Appl. Phys. A* **61**, 33.
Preuss, S. & Stuke, M. (1995). *Appl. Phys. Lett.* **67**, 338.
Samsonov, G.V. *Handbook of the Physicochemical Properties of the Elements.*
Santos, J.J. *et al.* (2002). *Phys. Rev. Lett.* **89**, 025001.
Sesame Report on Los Alamos Equation of State Library (1983). No. LALP-83-4, Los Alamos, NM.
Stuart, B.C. *et al.* (1995). *Phys. Rev. Lett.* **749**, 2248.
Zeldovich, Ya.B. & Raizer, Yu.P. (1967). *Physics of Shock Waves and High Temperature Hydrodynamic Phenomena,* Vol. 1. New York: Academic Press.